Fluorescence Reflectance Imaging of Macrophage-Rich Atherosclerotic Plaques Using an $\alpha_v\beta_3$ Integrin–Targeted Fluorochrome

Jens Waldeck*[1], Florian Häger*[1], Carsten Höltke[1,2], Christian Lanckohr[3], Angelika von Wallbrunn[1], Giovanni Torsello[4], Walter Heindel[1], Gregor Theilmeier[5], Michael Schäfers[2,6], and Christoph Bremer[1,6]

[1]Department of Clinical Radiology, University Hospital Muenster, University of Muenster, Muenster, Germany; [2]Department of Nuclear Medicine, University Hospital Muenster, University of Muenster, Muenster, Germany; [3]Department of Anesthesiology and Intensive Care Medicine, University Hospital Muenster, University of Muenster, Muenster, Germany; [4]St. Franziskus Hospital, Muenster, Germany; [5]Department of Anesthesiology, Medical University of Hannover, Hannover, Germany; and [6]Interdisciplinary Center for Clinical Research (IZKF Muenster, FG3 TH69 and ZPG 4b), University Hospital Muenster, University of Muenster, Muenster, Germany

Macrophages play an important role during the development and progression of atherosclerotic plaques. $\alpha_v\beta_3$ integrins are highly expressed by macrophages; thus, targeting $\alpha_v\beta_3$ may allow targeting of culprit macrophage-loaded atherosclerotic lesions *in vivo*. **Methods:** An $\alpha_v\beta_3$-targeted Arg-Gly-Asp (RGD) peptide was labeled with the cyanine 5.5 (Cy 5.5) dye and applied to image atherosclerotic plaques in apolipoprotein E–deficient mice. **Results:** The peptide–dye conjugate binds to $\alpha_v\beta_3$ integrin–positive RAW264.7 macrophages with high affinity. Competition experiments confirmed binding specificity of the probe. A significant fluorochrome accumulation in atherosclerotic plaques was demonstrated 24 h after injection by fluorescence reflectance imaging, which was blocked with high efficiency by competition with the unlabeled peptide. Conversely, the nonconjugated dye revealed only a minor fluorescence signal in the plaques. Fluorescence microscopy revealed colocalization of the probe with macrophages in the plaque of a mouse model for accelerated atherosclerosis, which was corroborated in human carotid artery specimens. In addition to macrophage-associated signals, binding of the probe to the neointima or elastica of the arteries was observed. **Conclusion:** RGD-Cy 5.5, combined with near-infrared optical imaging methods, allows the specific imaging of $\alpha_v\beta_3$-integrin expression on macrophages recruited to vascular lesions and may serve to estimate macrophage-bound inflammatory activity of atherosclerotic lesions.

Key Words: atherosclerotic plaque; optical imaging; $\alpha_v\beta_3$ integrin; RGD-Cy 5.5; fluorescence reflectance imaging

J Nucl Med 2008; 49:1845–1851
DOI: 10.2967/jnumed.108.052514

Atherosclerosis is a chronic inflammatory disease affecting the arterial vessel wall (atherosclerotic plaques). Atherosclerotic vascular lesions might progress into unstable plaques, which are prone to rupture, potentially resulting in occlusion of the affected vessel, which causes myocardial infarction or stroke. To target rupture-prone plaques therapeutically, imaging of the vessel wall, and especially of components of atherosclerotic plaques, is of increasing importance. Luminography (e.g., angiography) cannot sufficiently detect these lesions, because the plaque composition, not the resulting degree of stenosis, critically determines the stability of the lesion (*1*). Plaque rupture might occur in the course of plaque-weakening processes such as degradation of the fibrous cap by matrix metalloproteinases (MMPs) being secreted by the macrophages (*2*). MMPs have already been used as molecular targets for successful preclinical molecular imaging of atherosclerotic plaques (*3*). Lipid-rich macrophages are one of the main components of the lipid core of the plaque and contribute to plaque weakening and rupture and, by virtue of their high levels of membrane-bound tissue factor, to the resulting thrombotic vessel occlusion as well (*4*). Furthermore, active and dynamic recruitment of blood-derived monocytes/macrophages proportionally correlates with plaque lesion size and symptom severity (*5–8*). Interestingly, monocyte-derived macrophages express high levels of integrins. Molecular imaging of integrins may, therefore, allow for noninvasive assessment of macrophage infiltration (*9*). Moreover, integrins constitute an important class of cell-adhesion receptors responsible not only for cell–matrix and cell–cell adhesion but also for inside–out and outside–in signal transduction. Integrins are involved in a variety of biologic processes such as angiogenesis, thrombosis, inflammation, osteoporosis, cancer, and atherosclerosis (*10*). One of the most relevant integrins, $\alpha_v\beta_3$, is expressed on almost all cells originating from the mesenchyme and on

Received Mar. 8, 2008; revision accepted Jul. 2, 2008.
For correspondence or reprints contact: Jens Waldeck, Department of Clinical Radiology, University Hospital Muenster, University of Muenster, Haus Rosenbach, Waldeyerstrasse 1, 48149 Muenster, Germany.
E-mail: waldeck@uni-muenster.de
*Contributed equally to this work.

a variety of blood vessel cells (e.g., endothelial cells, smooth muscle cells [SMCs], fibroblasts, and platelets (*11*)) and binds to many different ligands, including several extracellular matrix proteins such as vitronectin, fibronectin, osteopontin, fibrinogen, and von Willebrand Factor (*12,13*). Specifically, the $\alpha_v\beta_3$ integrin is highly expressed in macrophages infiltrating atherosclerotic plaques and, along with membrane type-1 matrix metalloproteinases (MT-1 MMP), associates with the C terminus of the proteolytic active MMP-2 (*14,15*). This complex localizes MMP-associated proteolytic activity to the cell surface of, for example, macrophages, which may ultimately result in plaque destabilization.

The purpose of this study was to evaluate if the recently developed $\alpha_v\beta_3$-sensing, target-specific fluorophore Arg-Gly-Asp (RGD)–cyanine 5.5 (Cy 5.5) (*16*) binds to macrophages in atherosclerotic plaques and could thereby facilitate visualization of macrophage infiltration into plaques in a model of accelerated vascular lesion formation in apolipoprotein E–deficient ($ApoE^{-/-}$) knock-out mice, using near-infrared fluorescence reflectance imaging (FRI).

MATERIALS AND METHODS

Labeling of Cyclo[Cys-Arg-Gly-Asp-Cys]-Gly-Lys

Peptides were labeled as described elsewhere (*16*). Briefly, a cyclic RGD peptide was labeled with Cy 5.5 dye by the stirring of both educts in the dark, followed by high-performance liquid chromotography purification. As reported previously, the identity of the labeled product was confirmed by high-resolution electrospray mass spectrometry (*16*). Before intravenous application, the integrity of the tracer was checked using photometry and fluorometry (U3310 UV/VIS spectrophotometer and F-4500 fluorescence spectrometer, respectively; Hitachi).

Cell Lines

The mouse monocytic macrophagelike cell line RAW264.7 (TIB-71; American Type Culture Collection), human melanoma cells M21 (*16*), and human adenocarcinoma cell line MCF-7 (HTB-22; American Type Culture Collection) were cultured in RPMI 1640 (Invitrogen Corp.) supplemented with 10% fetal calf serum, penicillin, and streptomycin. M21 and MCF-7 cells were grown routinely in a monolayer culture at 37°C in a 5% CO_2 humidified air atmosphere. Murine peritoneal RAW264.7 cells were grown to 80% confluence at 37°C in a humidified atmosphere containing 5% CO_2 and 95% air, washed twice with fresh medium, recovered by scraping, and suspended in fresh medium at a density of 10^6/mL. Cell viability was checked via trypan blue (Sigma-Aldrich Chemie GmbH).

Fluorescence-Activated Cell Sorter (FACS) Analysis by Flow Cytometry

Cells were washed twice with phosphate-buffered saline (PBS) without Ca^{2+} and Mg^{2+} and harvested in 5 mL of ice-cold Versen buffer (13.7 mM sodium chloride [NaCl], 10 mM ethylenediaminetetraacetic acid, 2.6 mM potassium chloride, 8.1 mM sodium phosphate, and 1.4 mM potassium dihydrogen phosphate, pH 7.2). Aliquots of 2.5×10^5 cells were blocked with mouse IgG in PBS/bovine serum albumin (BSA; 0.1%) for 15 min at 4°C, washed twice with PBS with Ca^{2+} and Mg^{2+}, and resuspended in 150 μL of FACS binding buffer (cation buffer: 150 mM NaCl, 10 mM magnesium chloride, 10 mM calcium chloride, and 5 mM manganese chloride, pH 7.2, diluted to a concentration of 1:20 in PBS/0.1% BSA). The phycoerythrin-labeled murine monoclonal antibody 23C6-PE (3 μg/mL) (anti-$\alpha_v\beta_3$ complex [CD51/CD61]; Pharmingen) was added for 45 min at 4°C. Subsequently, cells were washed, resuspended in PBS/0.1% BSA, and analyzed on a Becton Dickinson FACSCalibur (BD Biosciences).

In Vitro Integrin $\alpha_v\beta_3$ Ligand-Binding Studies

Cells were seeded in 24-well plates. Confluent cells were washed twice with PBS and overlayed with 150 μL of binding buffer (cation buffer diluted to a concentration of 1:5 in 1% PBS). Afterward, 2 nmol RGD-Cy 5.5 was added into each well, incubated for 1 h at 37°C, washed twice with PBS, and covered with binding buffer. For predosing experiments, free RGD peptide (20 nmol) was added to each well for 45 min at 37°C. Vital cells were examined using a fluorescence microscope (TE 2000-S; Nikon) equipped with a mercury vapor lamp, 620/700-nm (excitation/emission) filters (AHF Analysentechnik AG), and a DXM1200F camera (Nikon).

Animal Model

$ApoE^{-/-}$ mice (CL 57/BL6; age, 12 wk; weight, 20–28 g) (Charles River) were anesthetized by an intraperitoneal injection of ketamine/xylazine (125/12.5 mg per kilogram of body weight), and the left common carotid artery was ligated using 5-0 silk (Ethicon GmbH) as described elsewhere (*17*). The animals were then fed a high-cholesterol diet (15% cocoa fat, 1.0% cholesterol, and 0.5% sodium cholate; Altromin GmbH & Co. KG) for 4 wk (Fig. 1). For near-infrared FRI, the Cy 5.5–labeled ligand (2 nmol/animal; $n = 3$) was injected via the tail vein. For tracer competition studies, mice were dosed with unlabeled peptide (20 nmol; $n = 3$) before tracer injection. To clarify unspecific biodistribution effects, nonmodified Cy 5.5 (2 nmol; $n = 3$) was injected into a cohort of animals. For fluorescence imaging, animals were euthanized 24 h after tracer injection and then perfused *in situ* with 0.9% NaCl (w/v) for 3 min (Fig. 1). The chest was opened to expose the heart (the aortic arch and the carotid arteries). Finally, the aortic arch and the carotid arteries were dissected from the heart and surrounding fat tissue. Macroscopic images were captured *in situ* with a Coolpix 4500 camera (Nikon) mounted on a Nikon binocular. Fluorescence reflectance images of supraaortic vessels were acquired *in situ* and after resection of the aortic arch including both carotid arteries. Subsequently, the dissected tissue was embedded in Tissue-Tek O.C.T. (Sakura), snap-frozen in liquid nitrogen, and serially sectioned (10 μm). Animal use was randomized to correct for interindividual lesion heterogeneity. The protocol was approved by the Institutional Animal Care Committee.

Immunohistochemistry

Mouse-Derived Tissues. Air-dried frozen sections were fixed in ice-cold acetone and blocked by incubation with 1% PBS/BSA for 30 min to prevent unspecific binding. Tissue sections were incubated with a monoclonal rat anti-mouse CD68 primary anti-

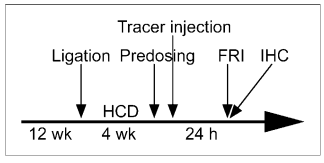

FIGURE 1. Timeline illustrating ligation, feeding, imaging, and postimaging examinations. HCD = high cholesterol diet; IHC: immunohistochemistry.

body (concentration, 1:100) (Clone FA-11; AbD Serotec) for 60 min at room temperature. A goat anti-rat Cy 3 antibody (Dianova) was applied as the secondary antibody (concentration, 1:100). Subsequently, slides were incubated with RGD-Cy 5.5 peptide for 60 min at room temperature before nuclear staining was performed using 4′,6-diamidino-2-phenylindole dihydrochloride (DAPI) (Sigma-Aldrich Chemie GmbH). Separate RGD-Cy 5.5 incubation was necessary, because fixation reduced RGD-Cy 5.5–derived fluorescence of the sections. Untreated sections exhibited RGD-Cy 5.5–derived fluorescence (data not shown). Tissue sections were captured with an Eclipse 50i microscope (Nikon) equipped with the DS 2MBWc digital camera (Nikon) and appropriate excitation/emission filters (AHF Analysentechnik AG).

Human-Derived Tissues. With the approval of the local ethics committee, human tissues were obtained during routine carotid artery endarterectomies. Specimens were stored in RNAlater solution (Ambion) and subsequently embedded in Tissue-Tek O.C.T. (Sakura). Air-dried frozen sections (10 μm) were fixed in ice-cold acetone. Unspecific binding was blocked using 1% PBS/BSA. Tissue sections were incubated for 60 min at room temperature using a monoclonal mouse anti-human CD68 primary antibody (concentration, 1:100) (Clone KP-1; DAKO Cytomation) and a goat anti-mouse Cy 3–labeled secondary antibody (concentration, 1:100) (Dianova) for 60 min at room temperature. Subsequently, slides were processed as described above.

FRI

Near-infrared FRI was performed using the In-Vivo FX Imaging System (Kodak Molecular Imaging Systems), equipped with a 150-W halogen illuminator with Cy 5.5 bandpass excitation (625 ± 18 nm) and emission filters (700 ± 17.5 nm). Fluorescence signals were captured with a 4-million-pixel cooled charge-coupled device camera equipped with a 10× zoom lens. Images were captured 24 h after probe injection, with an acquisition time of 60 s and identical window settings (e.g., f-stop, field of view). Fluorescence images were coregistered with the anatomic white-light images using MI 4.0 software (Kodak). Equal-sized regions of interest (≥1,500 pixels for each location) were placed within the highly visible plaque-like lesion, the adjacent carotid artery that was free of lesions, and the background (i.e., beside the animal). Contrast-to-noise ratios (CNRs) were determined as follows:

$$\mathrm{CNR} = \mathrm{signal}_{\mathrm{lesion}} - \mathrm{signal}_{\mathrm{normal\ artery}}/\mathrm{SD}_{\mathrm{background}}.$$

Statistical Analysis

All data are presented as mean values ± SEM. Statistical analysis of CNRs was conducted using 1-way ANOVA (GraphPad Instat, version 3.06; GraphPad Software Inc.) followed by post hoc analysis (Bonferroni). A P value of less than or equal to 0.05 was considered significant.

RESULTS

Peptide Labeling

After the cyclo[Cys-Arg-Gly-Asp-Cys]-Gly-Lys (RGD) peptide was labeled with the fluorophore Cy 5.5, a purity greater than or equal to 95% was achieved by reversed-phase high-performance liquid chromatography, with a retention time of 28.5 min. Yields of the RGD-Cy 5.5 conjugate were typically 75%−90% as calculated with $\varepsilon_{675} = 250{,}000\ (\mathrm{mol/L})^{-1}\mathrm{cm}^{-1}$ from the absorption spectrum measured with the PBS solution. The excitation and emission spectra of the targeted probe remained unchanged, compared with the nonmodified fluorophore showing an excitation peak at 675 nm and emission maximum at 694 nm.

FACS and Microscopic *In Vitro* Binding Studies

Flow cytometric and fluorescence microscopic binding studies were performed to determine the capacity of the cells to synthesize the $\alpha_v\beta_3$ integrin as well as the binding affinity of the tracer molecule for the target. FACS analysis revealed high $\alpha_v\beta_3$ expression levels in RAW264.7 and M21 cells, whereas $\alpha_v\beta_3$ integrin expression was virtually nonexistent in MCF-7 cells (data not shown). These results were confirmed by the cell assay *in vitro*. Cy 5.5–labeled RGD peptide distinctly bound to integrin-positive RAW and M21 cells (Supplemental Fig. 1; supplemental materials are available online only at http://jnm.snmjournals.org), whereas $\alpha_v\beta_3$-negative MCF-7 cells revealed no detectable level of cell-associated fluorescence. Incubation in advance with a 10-fold excess of the unlabeled peptide (140 μM) drastically reduced binding of the labeled tracer, proving specificity of the probe (Supplemental Fig. 1). Negligible signals were detected for all cell lines when they were incubated with the nonmodified Cy 5.5 dye (up to 140 μM; data not shown).

Near-Infrared FRI

Carotid artery ligation resulted in the formation of macrophage-rich vascular lesions proximal to the ligation in ApoE$^{-/-}$ mice ($n = 9$). RGD-Cy 5.5 strongly accumulated in the lesions (Fig. 2). RGD-Cy 5.5–derived signals were significantly stronger than with nonmodified Cy 5.5 and predosing experiments as visualized by high-resolution *ex vivo* FRI (Fig. 3). Autofluorescence of lesions was in the same range as background fluorescence derived from other tissues (data not shown). Thus, target-specific tracer binding can be assumed. Unspecific biodistribution effects of the unmodified Cy 5.5 seem, on the contrary, insignificant.

Semiquantitative assessment demonstrated the highest CNRs in RGD-Cy 5.5–injected mice (CNR, 88.8 ± 14.1, $n = 3$; Fig. 4), whereas predosing experiments ($n = 3$) efficiently decreased the CNR (34.2 ± 4.1). Free Cy 5.5 dye resulted in less than 20% of the RGD-Cy 5.5–mediated CNR (CNR, 15.8 ± 3.8).

Immunohistochemistry

To determine whether RGD-Cy 5.5 signals in vascular lesions were associated with macrophage infiltration, immunohistochemical stainings for the macrophage-specific antigen CD68 were performed (Supplemental Fig. 2). The RGD peptide–associated signal in the neointima colocalized with the macrophage-associated CD68 staining to a significant extent (Supplemental Fig. 2B). As expected, RGD-Cy 5.5 also stained the vascular SMCs and elastin-rich fibers (Supplemental Fig. 2D). Moreover, double

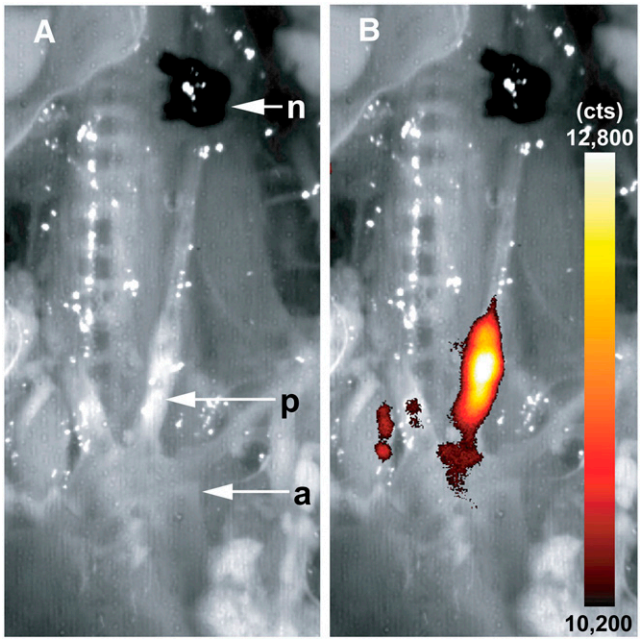

FIGURE 2. *In situ* fluorescence reflectance imaging overview of supraaortic vessels. FRI data were evaluated 24 h after intravenous injection of RGD-Cy 5.5 probe. Lesion formation (p) is clearly visible in bright field anatomic image (A). Fluorescence signals, given as photon counts per second (cts), emerged in area of lesion formation (B; merge of A with FRI data) proximal of ligation node (n). a = aortic arch.

stainings of human atherosclerotic plaques revealed distinct colocalization of $\alpha_v\beta_3$ and CD68 (Fig. 5D).

DISCUSSION

Progression and destabilization of atherosclerotic plaques with consecutive rupture is a critical process potentially resulting in life-threatening cardiovascular events such as myocardial infarction or stroke. Cellular processes such as monocyte-derived macrophage infiltration and enhanced MMP activation drive plaque instability (*4,18*). Although numerous studies explained the potential of targeting $\alpha_v\beta_3$ to image myocardial angiogenesis (e.g., of the healing myocardium after infarction (*19*)), we hypothesized that $\alpha_v\beta_3$ may be a suitable target to visualize atherosclerotic plaques because it is highly expressed on macrophages (*9*) and binds MMP-2 (*15*), a key molecule for plaque destabilization. Fluorochrome labeling of RGD peptides (*12,13,20*) and tumor targeting with optical probes using planar reflectance and 3-dimensional tomographic imaging methods have been shown to be feasible (*16,21*). The RGD tripeptid sequence is an integrin-shared adhesive motif (*22*) with distinct different affinities to Arg-Gly-Asp–dependent integrins such as $\alpha_v\beta_3$, $\alpha_5\beta_1$, or $\alpha_{IIb}\beta_3$ and led to the concept that different integrins distinguish varieties in the conformation and sequential environment of various RGD sites (*13,23–25*). Cyclization of the RGD peptide also increased binding with vitronectin receptors (i.e., $\alpha_v\beta_3$) dramatically but had no effect on the affinity to, for example, fibronectin receptors such as $\alpha_5\beta_1$ (*13,23, 26,27*). In this study, a Cy 5.5–labeled cyclic RGD peptide specifically binding $\alpha_v\beta_3$ integrins (*20*) was used to detect resident macrophages in vascular lesions in ApoE$^{-/-}$ mice. Because cyanine dyes are in part Food and Drug Administration approved (e.g., indocyanine green) or successfully applied in clinical studies, which is also true for RGD peptides, the toxicity of the construct for clinical applications should be negligible. Furthermore, cyclic RGD peptides are known to possess inhibitory concentrations of 50% ranging between 7 and 40 nmol/L for the inhibition of vitronectin to immobilized $\alpha_v\beta_3$ (*28*). A cystin moiety for cyclization was chosen because of the reported enhanced targeting efficiency of such peptides (*29,30*). *In vitro,* the probe tightly bound to viable murine RAW264.7 macrophages and $\alpha_v\beta_3$ integrin–positive M21 melanoma cells (*31,32*), suggesting a high $\alpha_v\beta_3$ receptor expression in macrophages. Binding of the RGD peptide to RAW macrophages was significantly reduced by dosing with the free cyclic peptide in advance, supporting target specificity of the probe.

On the basis of these data, RGD-Cy 5.5 was used for near-infrared FRI of macrophage-rich vascular lesions in the ligated left common carotid artery of ApoE$^{-/-}$ mice. This model differs from others in that it does not require mechanical trauma and widespread endothelial denudation to induce SMC proliferation. Notwithstanding, the carotid artery ligation model cannot exactly mimic the human pathophysiology. However, it emulates certain aspects of human vascular lesion formation, that is, macrophage and protease accumulation (*33*). Our results highlighted the capability of the Cy 5.5–labeled RGD peptide to specifically image $\alpha_v\beta_3$ expression in those vascular lesions because the fluorescence signal could be efficiently blocked in competition experiments. Nontargeted cyanine dyes did not show any relevant fluorochrome retention in the lesions. In addition, fluorescence signals were detected at the site of surgery (Fig. 3) distal to the arterial ligation. This may well reflect postsurgical inflammatory processes. However, the CNRs of the RGD-Cy 5.5 signals within the lesion were unambiguously higher than CNRs from tracer competition experiments or when unlabeled cyanine dye was used. Thus, simple nonspecific biodistribution effects of the cyanine dye can be excluded. Immunohistochemistry confirmed that FRI signals were due to accumulation of the tracer in $\alpha_v\beta_3$-expressing macrophages. We used a specific antibody against the 110-kDa transmembrane glycoprotein CD68, specific for monocytes and tissue macrophages (*34*), and restricted staining to macrophages within the neointima. RGD-Cy 5.5 not only strongly stained macrophages but also revealed a weaker signal associated with elastin-rich fibers of the medium and vascular SMCs underlying the atherosclerotic plaque. These results were also congruent to the findings of Antonov et al. (*9*), who demonstrated that $\alpha_v\beta_3$ integrin receptors, compared with endothelial cells, SMCs, and tissue macrophages, were highly upregu-

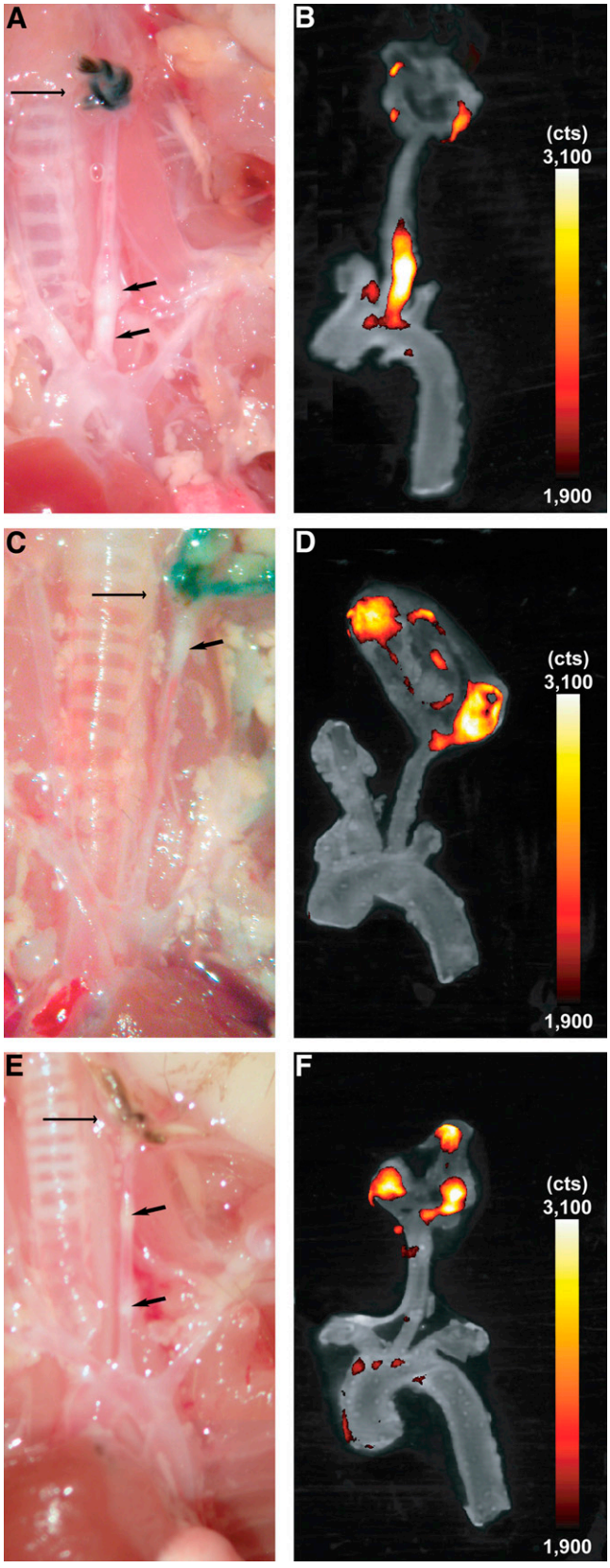

FIGURE 3. FRI of resected carotid artery in different experimental groups. ApoE$^{-/-}$ mice were injected with either RGD-Cy 5.5 (A and B), free RGD peptide before tracer injection (C and D), or free Cy 5.5 (E and F). Arrows on macroscopic images (A, C, and E) indicate vascular lesions (short arrow) and ligation (long arrow). (B, D, and F) Overlay of color-encoded near-infrared fluorescence images of resected arteries and corresponding white-light images. Fluorescence intensity is given in photon counts per second (cts). Strong fluorescence signal was observed at plaques of left carotid artery using Cy 5.5–labeled RGD peptide (B), which corresponds well with visible atherosclerotic lesion (A). Dosing in advance reveals artifical fluorescence signal at site of surgery but no relevant fluorescence within plaque (D). Free Cy 5.5 resulted in weak signal in plaque (F). For CNR calculation, images were processed and windowed identically.

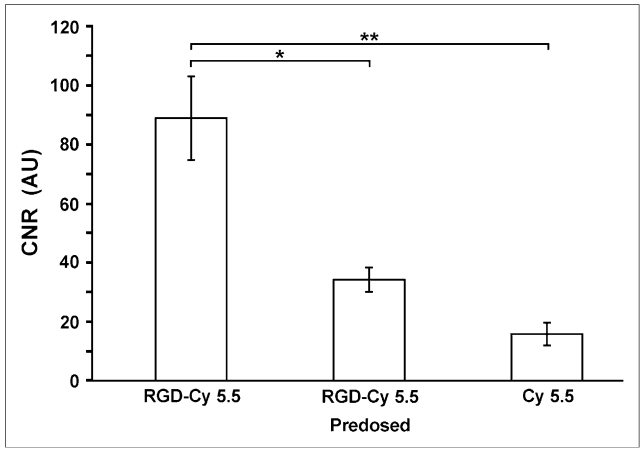

FIGURE 4. Semiquantitative FRI results for all experimental groups. Calculated CNRs were 88.8 (±14.1 [SEM]) for RGD-Cy 5.5–injected animals, which could be significantly reduced by advance dosing with free peptide (CNR, 34.2 ± 4.1). Free Cy 5.5 revealed only weak fluorescence signals (CNR, 15.8 ± 3.8). *$P < 0.05$; **$P < 0.01$. AU = arbitrary units.

lated in atheroma macrophages of early lipid (fatty streak) and advanced atherosclerotic lesions. However, endothelial cells and SMCs are known to express the vitronectin receptor on their surface (*11*) and to bind proteolytically active MMP-2, among other ligands. Assuming a migratory phenotype (*15*), RGD-Cy 5.5 binding to these cells is expected and may potentially dilute the signal-to-noise ratio of the macrophages but may actually add to the sensitivity of lesion detection in vascular imaging approaches. Immunohistochemistry on the human carotid endarterectomy specimen confirmed high expression levels of the target in human atherosclerotic plaques and colocalization with CD68-positive macrophages. Although other cell types and extracellular matrix components did exhibit some binding of the probe, the macrophage-bound RGD-Cy 5.5 signal was much stronger and readily distinguishable, suggesting that $\alpha_v\beta_3$ targeting may be a viable concept for translation from bench to bedside.

Furthermore, this tracer might be applicable in angiogenesis imaging for risk stratification of patients after myocardial infarction, because $\alpha_v\beta_3$ is barely detectable

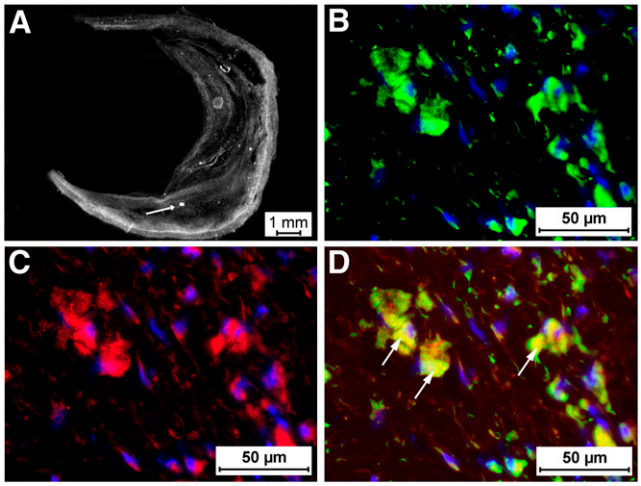

FIGURE 5. Immunohistochemistry of human atherosclerotic plaques. Human carotid endarterectomy specimens (A, white light) were stained for CD68 (B and D; green signal) and RGD-Cy 5.5 (C and D; red signal). Nuclei were counterstained with 4′,6-diamidino-2-phenylindole (DAPI; B, C, and D; blue signal). (D) Merged image of macrophages (arrows) within plaque demonstrated CD68 and RGD-Cy 5.5 double staining, suggesting that macrophage infiltration may potentially be imaged in humans using this approach. Box and arrow indicate the enlargement shown in B–D. Scale bars are indicated.

in endothelial cells in the quiescent state but shows high expression in vascular endothelial cells during angiogenesis (*35,36*).

In general, optical imaging is an attractive concept for the detection of molecular signatures *in vivo* because of its exquisite sensitivity, which is comparable to scintigraphic imaging techniques (*37*). In the near-infrared range, good tissue penetration and low background signal allow fluorochromes to be detected, even in the pico- to femtomolar range. Potential clinical applications of this optical imaging technology for cardiovascular diseases are conceivable. More recently, imaging techniques such as optical coherence tomography have successfully been explored clinically for characterization of coronary artery plaques using a catheter-based imaging approach (*38*). The RGD-Cy 5.5 tracer tested in this work might be usable in combination with optical coherence tomography to identify plaque rupture, fibrous cap erosion, intracoronary thrombi, and thin cap fibroatheroma, because with planar fluorescence imaging techniques such as FRI a sufficient correlation between fluorescence signal and anatomic fluorescence origin is hard to establish. Thus, thorax opening was necessary in our approach. However, optical coherence tomography offers exquisite anatomic resolution in the micromolar range and might allow *in vivo* microscopic resolution of structural signatures related to plaque destabilization. This technique may provide the chance to specifically determine plaque dignity significantly earlier than with the available technologies, which are capable of imaging only plaque morphology at best. From a technical point of view, near-infrared imaging technology can be miniaturized just like optical coherence tomography so that a clinical translation could be straightforward. Indeed, quantitative real-time catheter-based fluorescence imaging has most recently been described for laparoscopic and colonoscopic applications in mice so that the grounds for translation of this technology for intravascular applications are prepared (*39*). Thus, near-infrared imaging combined with a target-specific probe as shown in this study may potentially further enhance the diagnostic potential of invasive coronary angiography. Moreover, incorporation of FRI techniques into ultrasoundlike, handheld devices has been proposed, opening avenues to apply near-infrared imaging for characterization of superficial artery segments (e.g., carotid artery) or intraprocedural applications of the technology (*40*).

CONCLUSION

This study demonstrates that macrophage-associated $\alpha_v\beta_3$ integrin expression can be visualized using FRI approaches. This imaging technique is, therefore, a versatile tool not only for experimental small-animal molecular imaging but also potentially for noninvasive target detection, for example, for clinical plaque imaging in future imaging applications.

ACKNOWLEDGMENTS

We thank Susanne Greese, Wiebke Gottschlich, Dr. Julia Heselhaus, Irmgard Hoppe, and Ingrid Otto-Valk for their technical assistance and Bodo Levkau for providing the macrophage cell line. This work was supported in part by the Deutsche Forschungsgesellschaft (BR 1653/2-1, SFB 656 project A1, A4, Z2), Interdisciplinary Center for Clinical Research (FG3, The1/068/04, ZPG 4b), and European Community (IP 6th framework, Molecular Imaging and Network of Excellence DiMI).

REFERENCES

1. Theilmeier G, Quarck R, Verhamme P, et al. Hypercholesterolemia impairs vascular remodelling after porcine coronary angioplasty. *Cardiovasc Res.* 2002;55:385–395.
2. Martinet W, De Meyer GR. Selective depletion of macrophages in atherosclerotic plaques: myth, hype, or reality? *Circ Res.* 2007;100:751–753.
3. Schafers M, Riemann B, Kopka K, et al. Scintigraphic imaging of matrix metalloproteinase activity in the arterial wall in vivo. *Circulation.* 2004;109:2554–2559.
4. Libby P, Ridker PM. Inflammation and artherothrombosis: from population biology and bench research to clinical practice. *J Am Coll Cardiol.* 2006;48(suppl A):A33–A46.
5. MacNeill BD, Jang IK, Bouma BE, et al. Focal and multi-focal plaque macrophage distributions in patients with acute and stable presentations of coronary artery disease. *J Am Coll Cardiol.* 2004;44:972–979.
6. Lessner SM, Prado HL, Waller EK, Galis ZS. Atherosclerotic lesions grow through recruitment and proliferation of circulating monocytes in a murine model. *Am J Pathol.* 2002;160:2145–2155.
7. Swirski FK, Libby P, Aikawa E, et al. Ly-6Chi monocytes dominate hypercholesterolemia-associated monocytosis and give rise to macrophages in atheromata. *J Clin Invest.* 2007;117:195–205.
8. Swirski FK, Pittet MJ, Kircher MF, et al. Monocyte accumulation in mouse atherogenesis is progressive and proportional to extent of disease. *Proc Natl Acad Sci USA.* 2006;103:10340–10345.

9. Antonov AS, Kolodgie FD, Munn DH, Gerrity RG. Regulation of macrophage foam cell formation by $\alpha_V\beta_3$ integrin: potential role in human atherosclerosis. *Am J Pathol.* 2004;165:247–258.
10. Meyer A, Auernheimer J, Modlinger A, Kessler H. Targeting RGD recognizing integrins: drug development, biomaterial research, tumor imaging and targeting. *Curr Pharm Des.* 2006;12:2723–2747.
11. Kokubo T, Uchida H, Choi ET. Integrin $\alpha_v\beta_3$ as a target in the prevention of neointimal hyperplasia. *J Vasc Surg.* 2007;45(suppl):A33–A38.
12. Cheresh DA, Spiro RC. Biosynthetic and functional properties of an Arg-Gly-Asp-directed receptor involved in human melanoma cell attachment to vitronectin, fibrinogen, and von Willebrand factor. *J Biol Chem.* 1987;262:17703–17711.
13. D'Souza SE, Ginsberg MH, Matsueda GR, Plow EF. A discrete sequence in a platelet integrin is involved in ligand recognition. *Nature.* 1991;350:66–68.
14. Brooks PC, Stromblad S, Sanders LC, et al. Localization of matrix metalloproteinase MMP-2 to the surface of invasive cells by interaction with integrin αv β3. *Cell.* 1996;85:683–693.
15. van Hinsbergh VW, Engelse MA, Quax PH. Pericellular proteases in angiogenesis and vasculogenesis. *Arterioscler Thromb Vasc Biol.* 2006;26:716–728.
16. von Wallbrunn A, Höltke C, Zuhlsdorf M, Heindel W, Schäfers M, Bremer C. In vivo imaging of integrin $\alpha_v\beta_3$ expression using fluorescence-mediated tomography. *Eur J Nucl Med Mol Imaging.* November 28, 2006 [Epub ahead of print].
17. Ivan E, Khatri JJ, Johnson C, et al. Expansive arterial remodeling is associated with increased neointimal macrophage foam cell content: the murine model of macrophage-rich carotid artery lesions. *Circulation.* 2002;105:2686–2691.
18. Chung A, Gao Q, Kao WJ. Macrophage matrix metalloproteinase-2/-9 gene and protein expression following adhesion to ECM-derived multifunctional matrices via integrin complexation. *Biomaterials.* 2007;28:285–298.
19. Jaffer FA, Sosnovik DE, Nahrendorf M, Weissleder R. Molecular imaging of myocardial infarction. *J Mol Cell Cardiol.* 2006;41:921–933.
20. Ruoslahti E, Pierschbacher MD. New perspectives in cell adhesion: RGD and integrins. *Science.* 1987;238:491–497.
21. Chen X, Conti PS, Moats RA. In vivo near-infrared fluorescence imaging of integrin alphavbeta3 in brain tumor xenografts. *Cancer Res.* 2004;64:8009–8014.
22. Schraa AJ, Kok RJ, Moorlag HE, et al. Targeting of RGD-modified proteins to tumor vasculature: a pharmacokinetic and cellular distribution study. *Int J Cancer.* 2002;102:469–475.
23. D'Souza SE, Ginsberg MH, Plow EF. Arginyl-glycyl-aspartic acid (RGD): a cell adhesion motif. *Trends Biochem Sci.* 1991;16:246–250.
24. Pfaff M, Tangemann K, Muller B, et al. Selective recognition of cyclic RGD peptides of NMR defined conformation by αIIbβ3, αVβ3, and α5β1 integrins. *J Biol Chem.* 1994;269:20233–20238.
25. Yamada KM. Adhesive recognition sequences. *J Biol Chem.* 1991;266:12809–12812.
26. Pierschbacher MD, Ruoslahti E. Influence of stereochemistry of the sequence Arg-Gly-Asp-Xaa on binding specificity in cell adhesion. *J Biol Chem.* 1987; 262:17294–17298.
27. Haubner R, Wester HJ, Reuning U, et al. Radiolabeled $\alpha_v\beta_3$ integrin antagonists: a new class of tracers for tumor targeting. *J Nucl Med.* 1999;40:1061–1071.
28. Janssen ML, Oyen WJ, Dijkgraaf I, et al. Tumor targeting with radiolabeled $\alpha_v\beta_3$ integrin binding peptides in a nude mouse model. *Cancer Res.* 2002;62: 6146–6151.
29. Colombo G, Curnis F, De Mori GM, et al. Structure-activity relationships of linear and cyclic peptides containing the NGR tumor-homing motif. *J Biol Chem.* 2002;277:47891–47897.
30. Yamada T, Uyeda A, Kidera A, Kikuchi M. Functional analysis and modeling of a conformationally constrained Arg-Gly-Asp sequence inserted into human lysozyme. *Biochemistry.* 1994;33:11678–11683.
31. Haubner R, Bruchertseifer F, Bock M, Kessler H, Schwaiger M, Wester HJ. Synthesis and biological evaluation of a ^{99m}Tc-labelled cyclic RGD peptide for imaging the $\alpha_v\beta_3$ expression. *Nuklearmedizin.* 2004;43:26–32.
32. Haubner R, Wester HJ, Burkhart F, et al. Glycosylated RGD-containing peptides: tracer for tumor targeting and angiogenesis imaging with improved biokinetics. *J Nucl Med.* 2001;42:326–336.
33. Xu Q. Mouse models of arteriosclerosis: from arterial injuries to vascular grafts. *Am J Pathol.* 2004;165:1–10.
34. Holness CL, Simmons DL. Molecular cloning of CD68, a human macrophage marker related to lysosomal glycoproteins. *Blood.* 1993;81:1607–1613.
35. Brooks PC, Clark RA, Cheresh DA. Requirement of vascular integrin alpha v beta 3 for angiogenesis. *Science.* 1994;264:569–571.
36. Meoli DF, Sadeghi MM, Krassilnikova S, et al. Noninvasive imaging of myocardial angiogenesis following experimental myocardial infarction. *J Clin Invest.* 2004;113:1684–1691.
37. Persigehl T, Heindel W, Bremer C. MR and optical approaches to molecular imaging. *Abdom Imaging.* 2005;30:342–354.
38. Kubo T, Imanishi T, Takarada S, et al. Assessment of culprit lesion morphology in acute myocardial infarction: ability of optical coherence tomography compared with intravascular ultrasound and coronary angioscopy. *J Am Coll Cardiol.* 2007;50:933–939.
39. Upadhyay R, Sheth RA, Weissleder R, Mahmood U. Quantitative real-time catheter-based fluorescence molecular imaging in mice. *Radiology.* 2007;245: 523–531.
40. Ntziachristos V, Tung CH, Bremer C, Weissleder R. Fluorescence molecular tomography resolves protease activity in vivo. *Nat Med.* 2002;8:757–760.